Vol. 15: 109–122, 2000 | CLIMATE RESEARCH Clim Res | Published July 20

Changing cyclones and surface wind speeds over the North Atlantic and Europe in a transient GHG experiment

P. Knippertz*, U. Ulbrich, P. Speth

Institute of Geophysics and Meteorology, University of Cologne, Kerpener Str. 13, 50923 Köln, Germany

ABSTRACT: A 240 yr run of the ECHAM4/OPYC3 coupled ocean-atmosphere model with transient greenhouse gas (GHG) forcing according to the IPCC IS92a scenario is examined with respect to simulated changes in boreal winter cyclone activity and 10 m wind speeds over Europe, the North Atlantic and Eastern North America. It is found that simulated cyclone activity undergoes a pronounced north- and eastward shift over Europe and the Northeast Atlantic. This shift is accompanied by a decrease in the number of weak cyclones and an increase in deep cyclones (with core pressures below 970 hPa) in this area. The cyclone signal corresponds to the changes in storm track activity and upper-tropospheric baroclinicity. Increases of mean wind speeds and of wind speed extremes are identified over Northern Europe and parts of the East Atlantic. The wind signal is due to an increase in wind speed variability and an intensification of the westerly mean current connected with an enhanced mean pressure gradient. It is shown that the rising number of extreme wind events in the GHG simulation is connected to the augmented occurrence of deep cyclones over Northern Europe and the adjacent ocean areas. There are also strong wind speed increases over Hudson Bay and the Greenland Sea. They are restricted to the planetary boundary layer and appear to be connected to the reduction in winter mean sea-ice cover, which leads to locally decreased static stability and—over the Greenland Sea—also to a reduction in surface roughness.

KEY WORDS: GCM · GHG scenario · Cyclones · Low-level wind extremes · Storm tracks · Baroclinicity

1. INTRODUCTION

Cyclones and their associated frontal weather systems are important features of European climate. The frequency and strength of cyclones have a marked influence on the variability of surface wind speed, a quantity of high economic relevance. Mean winds are important for wind energy and wave heights, which affect ocean shipping and off-shore industries (WASA-Group 1998; WASA: Waves and Storms in the North Atlantic); extreme winds can lead to large economic losses and even loss of life (Schraft et al. 1993). Apart from floodings (Penning-Rowsell et al. 1996), extreme winds are in fact the most important hazard of mid-latitude wintertime depressions (Munich Re 1977, 1990). In the early 1990s Western, Central and Northern Europe were hit by a number of strong winter storms; the ones in 1990 alone caused economic losses of about US $15 billion (Dorland et al. 1996).

These storms and the large number of deep cyclones in the late 1980s and early 1990s stimulated research on this issue. With respect to the occurrence of deep cyclones, there is general agreement on an increase in recent years (Dronia 1991, Schinke 1993, Stein & Hense 1994, Haak & Ulbrich 1996, Lambert 1996, Schmith et al. 1998). With respect to the occurrence of extreme wind events, this issue is less certain, mainly because of data inhomogeneity in wind measurements and the high variability on decadal time scales of this quantity (von Storch et al. 1993, Kaas et al. 1996). The WASA-Group (1998) investigated wave climate as an indirect indicator of wind velocity. They observed a roughening in the northeast Atlantic and in the North

*E-mail: knippertz@meteo.uni-koeln.de

Sea for the recent decades, but according to their estimates the current intensity is not larger than it was at the beginning of this century.

Assuming a trend in storm and cyclone occurrence is detectable in observational data, it would be interesting if the observed changes are part of natural variability or if they can be assigned to rising greenhouse gas (GHG) concentrations. This question is generally addressed by investigating numerical climate simulations with a prescribed increase in GHG forcing. There is a certain agreement between different simulations of this kind concerning the signal in the mean state of the climate system, particularly with regard to the vertical meridional structure of temperature change (Mitchell et al. 1990, Karoly et al. 1994, IPCC 1996, Cubasch et al. 1997). Warming maxima in the low-latitude upper troposphere and in the polar lower troposphere are common features of many GHG simulations. These temperature changes lead to increased upper tropospheric and reduced lower tropospheric zonal mean baroclinicity and to a global increase in atmospheric water-vapour content.

Although studies with simplified conceptional models have shown that baroclinic wave activity is more sensitive to lower than to upper level changes (Held & O'Brien 1992, Pavan 1996, Lunkeit et al. 1998), it is not a straightforward task to predict the net effect of the described baroclinicity signal on synoptic activity. The influence of the increased water-vapour content on baroclinic wave activity is also not clear. Several studies (Golding 1984, Gutowski et al. 1992, Fantini 1993) reveal that activity is intensified due to an additional latent heat release in the synoptic systems. Held (1993), however, argues that a larger efficiency of mid-latitude eddies in transporting heat meridionally requires weaker or fewer cyclones to balance the global water and energy budget. In addition, the zonal inhomogeneity of the changes makes this issue even more complex. Therefore the net effect of the described temperature change on the occurrence and intensity of cyclones and low-level wind speed is still a matter of scientific debate.

Thus, in order to estimate how increasing GHG concentrations affect the frequency and intensity of cyclones and strong winds in Europe, changes in synoptic activity as simulated by a complex general circulation model (GCM) must be considered. There have been a variety of studies on the CO_2 signal of baroclinic activity measured in terms of the standard deviation of the bandpass filtered variability of the 500 hPa geopotential height, simply called 'storm track activity' (Stephenson & Held 1993, Hall et al. 1994, Lunkeit et al. 1996, Beersma et al. 1997, Cubasch et al. 1997, Zhang & Wang 1997, Ulbrich & Christoph 1999). In addition, there have been studies on changes in cyclone frequency and intensity (König et al. 1993, Lambert 1995, Lunkeit et al. 1996, Beersma et al. 1997, Zhang & Wang 1997, Carnell & Senior 1998, Schubert et al. 1998). Only a few studies have explicitly considered changes of low-level wind speed in GHG simulations (e.g. Carnell et al. 1996, Lunkeit et al. 1996, Zwiers & Kharin 1998), partly because of the missing of details in orography, surface roughness, etc., that are important for this quantity on a local basis. This problem can be approached by the application of different downscaling techniques (statistical; dynamical, see e.g. Mengelkamp 1999). Since all these approaches make use of the simulated large-scale fields, a regionalization cannot substantially alter the basic changes produced by the GCM (Machenhauer et al. 1998). Therefore a careful analysis of the simulated large-scale winds should be performed before regionalization attempts are made.

In this paper we address changes in boreal winter synoptic activity and low-level mean and extreme wind speeds over Europe, the North Atlantic and Eastern North America as simulated in a transient GHG experiment with the coupled model ECHAM4/OPYC3. Section 2 of this paper gives a short description of the data and the model. In Section 3 local changes in mean and extreme 10 m wind speed will be investigated in the light of simulated changes in mean sea-level pressure (MSLP) and surface cyclone occurrence. Changes in these quantities as well as in storm track activity and lower and upper level baroclinicity are presented. After an investigation of the relation between strong wind events and cyclones and the role of sea-ice for the wind signal in Sections 4 and 5, a discussion of the results and conclusions are given in Section 6.

2. DATA

We consider data from a 240 yr transient GHG experiment conducted with the coupled GCM ECHAM4/OPYC3. The atmospheric model has a spectral resolution of T42 and uses a hybrid vertical coordinate system with 19 irregularly spaced levels that are terrain following at the surface and coincide with pressure at the uppermost level at 10 hPa. Nonlinear terms and most of the parameterized physics are calculated on the associated Gaussian transform grid which has a resolution of about 2.8° × 2.8° in latitude and longitude. For a detailed description of the atmospheric model see Roeckner et al. (1992, 1996a).

The oceanic component is the OPYC (Ocean on isoPYCnal coordinates) model (Oberhuber 1993), which consists of sub-models for the interior ocean, the surface mixed layer and for sea-ice. The model has 11 layers. Poleward of 36°, the horizontal resolution is

identical to that of the atmospheric model. At lower latitudes, the meridional grid spacing is gradually decreased down to 0.5° at the equator. The model components are coupled quasi-synchronously and exchange information about surface fluxes of momentum, heat, freshwater, etc., and sea-surface temperature and sea-ice variables once a day. More details on the coupling technique and on the performance of the model can be found in Roeckner et al. (1996b) and Bacher et al. (1998). The anthropogenic GHG forcing is prescribed using observed data between 1860 and 1990, and the IS92a scenario (IPCC 1992) afterwards. In this simulation the individual GHGs are treated separately with regard to their contribution to the net radiative forcing. Effects from sulphate aerosols and tropospheric ozone are not taken into account. The model simulation is initialized with present-day values rather than pre-industrial ones. This causes a warm bias in the initial state of the scenario run which is maintained throughout the simulation and is regarded to have negligible impact on climatic trends (Roeckner et al. 1998). Further details on this simulation are given in Roeckner et al. (1998).

As the GHG concentrations increases slowly during the first decades of the run, the period between 1880 and 1930 represents present-day conditions and is subsequently called the 'control period'. The GHG signal is determined by a comparison to a 50 yr period out of the final part of the simulation (Years 2039 to 2089, subsequently called the 'scenario period'), when the CO_2 concentrations have about doubled to tripled. The control period was preferred to the actual control run as a reference climate state, because we intended to analyse the response of the model to the additional GHGs within the transient run.

The significance of the change (differences between the 2 periods) is calculated with a simple 2-sided *t*-test applied to the variances of the winter-to-winter variability. Because of the strong nonlinear trend in the GHG concentrations and the forcing at the end of the run, the second period cannot be considered homogeneous, since the trend enlarges the standard deviation with respect to the 50 winter mean. The results of the *t*-test must therefore be regarded as a pessimistic estimation of the 'real' significances. In order to take the nonlinearity of the forcing into consideration, part of our analysis of the climate signal is based on the nonlinear trends in time series of winter means over the complete run rather than on differences between the two 50 yr periods.

We took only winter (December, January, February) periods into account as the occurrence of strong storm events in the Atlantic/European area is concentrated in this season (for extreme cyclone events see e.g. Haak & Ulbrich 1996). The 10 m wind data is only available as 12 hourly averages. We use these values not only for mean wind computations but also as a proxy for extreme wind occurrence. Consequently, the actual value of extremes in wind speed events are not optimally caught, but the averaged fields give a good spatial representation of storm affected areas. We compared the upper first percentiles (the threshold dividing the highest 1% from the rest of the statistical ensemble) of the 10 m, 12 hourly means with the 2 m, 12 hourly maximum wind speed and found an agreement in the structure of both the absolute fields and the climate signal, except that the maximum wind speed field is more noisy. As the MSLP and other low-level fields are rather unrealistic over Greenland, we blanked this area out in all figures that show low-level quantities.

3. CO_2-INDUCED CHANGES

3.1. MSLP and baroclinicity

The wintertime MSLP climatology from the NCEP (National Centers for Environmental Prediction) re-analysis (Fig. 1a) shows a minimum of just below 1000 hPa between the southern tip of Greenland and Iceland and a broad maximum reaching from the Atlantic southwest of the Azores to the Iberian Peninsula and into Northern Africa. The position and depth of the climatological Icelandic Low are well reproduced in the model's control period (Fig. 1b). The deviation in central pressure is only about 1 hPa. In contrast, the Azores High is shifted to the northeast and reaches a maximum pressure that is about 5 hPa higher than in the NCEP re-analysis. Consequently, the mean pressure gradient is somewhat higher over Western and Central Europe in the simulations than in the re-analysis.

The comparison of the control and the scenario period indicates a strong and statistically significant decrease (up to 6 hPa) of MSLP at high latitudes in the area considered (Fig. 1c). Weakly enhanced pressure is found over Southern and Western Europe leading to an increased mean pressure gradient in Northern and Central Europe and a strengthening of the mean westerly winds. This signal structure is in good agreement with the results from a nonlinear trend analysis performed by Ulbrich & Christoph (1999) for the same model simulation.

Surface cyclone activity and upper air storm track are related to baroclinic instability, which can be quantified in terms of the maximum Eady growth rate (see Eady 1949, Lindzen & Farrell 1980, Hoskins & Valdes 1990). It is defined as $\sigma_{BI} = 0.31(f/N)|\delta v/\delta z|$, where f is the Coriolis parameter, N is the static stability, z is the vertical coordinate and v is the horizontal wind vector. This quantity was calculated from monthly means of temperature, geopotential height and wind both for

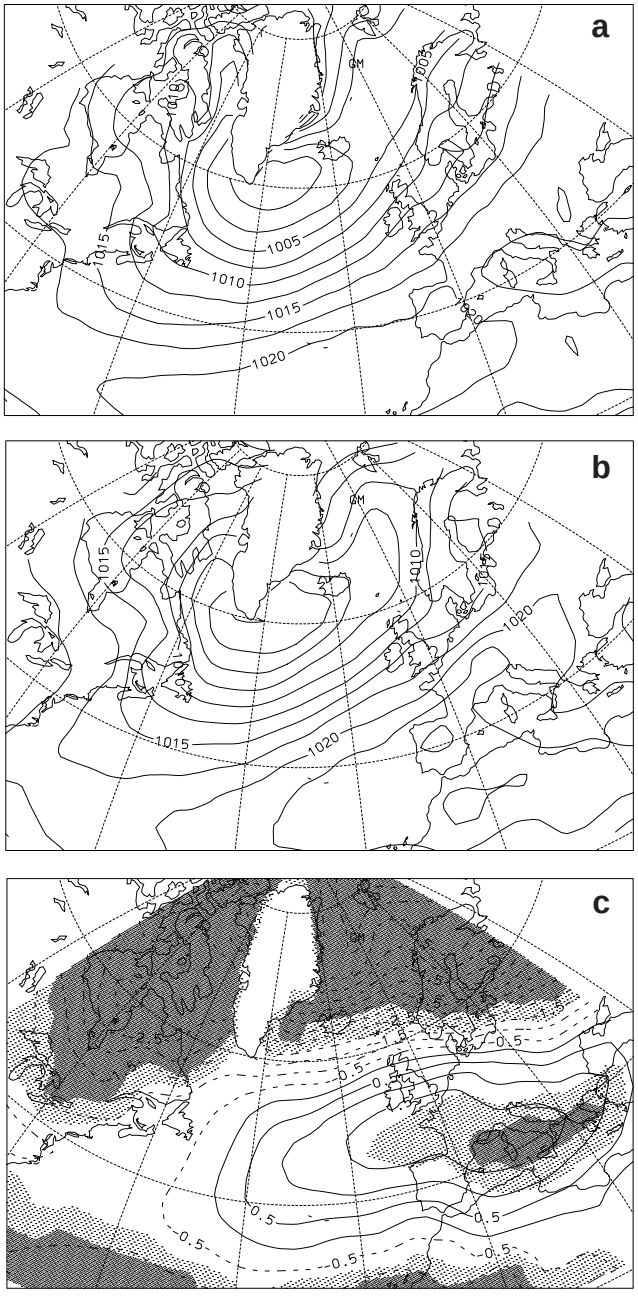

Fig. 1. Winter (DJF) mean sea level pressure. (a) NCEP re-analysis, 1958/59 to 1996/97; (b) control period; and (c) scenario – control period. Isoline spacing is 2.5 hPa in (a) and (b) and 0.5 hPa in (c). Light and dark shading in (c) indicates statistical significance at the 5% and 1% levels, respectively (with respect to a local *t*-test)

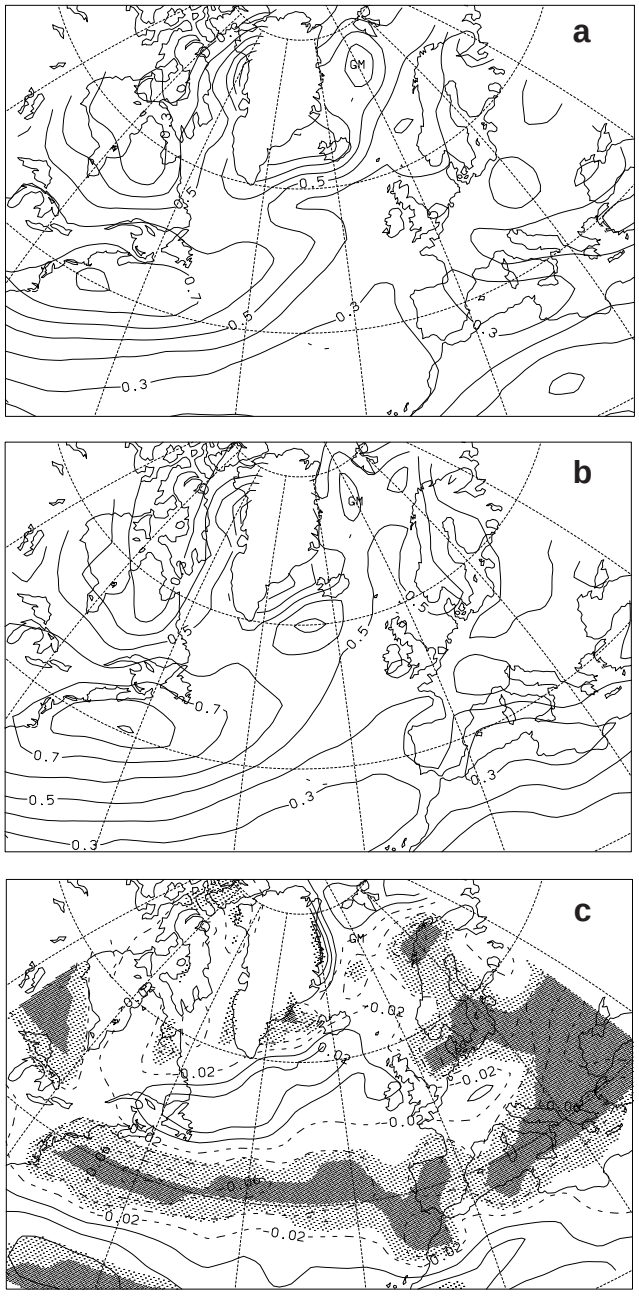

Fig. 2. Winter (DJF) mean maximum Eady growth rate for the 700 to 850 hPa layer. (a) NCEP re-analysis, 1949/50 to 1995/96; (b) control period; and (c) scenario – control period. Isoline spacing is 0.1 d^{-1} in (a) and (b) and 0.02 d^{-1} in (c). Light and dark shading in (c) indicates statistical significance at the 5% and 1% levels, respectively (with respect to a local *t*-test)

the lower (850 to 700 hPa) and the upper troposphere (500 to 300 hPa). The winter mean lower tropospheric baroclinicity from the NCEP re-analysis shows a distinct maximum off the east coast of North America and a zone of relatively high baroclinicity stretching over the Atlantic into Northern Europe (Fig. 2a). This is in good agreement with the winter mean from the control period (Fig. 2b). In both the model (Fig. 3b) and the climatology (Fig. 3a) the upper tropospheric maximum of the Eady parameter has a more southwesterly location

than its lower tropospheric counterpart. The comparison of the winter mean of the control period with the climatology reveals a good agreement in the overall structure of the fields, except for a westward shift of the maximum in the model accompanied by somewhat too high values over the North Atlantic.

With increased GHG concentrations, the reduction of the lower tropospheric meridional temperature gradient and land-sea contrasts leads to a decreased baroclinicity over most of the North Atlantic and Europe. There is, however, no significant change in the area of maximum baroclinicity, which reaches from Newfoundland to Ireland (Fig. 2c). In the upper troposphere, the change of mean temperatures induces a northward shift and a downstream extension of the zone of high baroclinicity. The increasing upper tropospheric baroclinicity over the Greenland, Iceland and Norwegian Sea (Fig. 3c) will contribute to better conditions for cyclones to intensify in this region and to move further into Northern Europe, particularly since there is no opposing signal in the lower tropospheric baroclinicity over this region. Thus, the changes in baroclinicity could contribute to an increased activity of cyclones and upper air storm track downstream of the present day climatological maximum as discussed in the following sections of this paper.

3.2. Cyclone frequency and depth

Cyclone core positions and pressures were identified by means of an automatic identification routine (Haak & Ulbrich 1996). The scheme uses 1000 hPa geopotential height data. The core pressures are calculated from the height values of the minima by means of the barometric height equation. In order to smooth the frequency distribution, cyclone cores are counted in $10° \times 10°$ grid boxes for different core pressure ranges every time step (12 h). Consequently, a cyclone is counted more than once if it lasts longer than 12 h. For the control climate cyclone frequency distribution for core pressures less than 1000 hPa and less than 970 hPa (Figs. 4b & 5b) both show pronounced maxima over the North Atlantic. A comparison with climatologies obtained from the ECMWF re-analysis for 1978/1979 to 1993/94 with the same identification routine (Figs. 4a & 5a) shows good agreement in structure. The number of cyclones with core pressures less than 970 hPa per winter is underestimated by about 50%. This result may be explained from the higher resolution of the re-analysis data, which allows for more distinct local extremes and sharper local pressure gradients to occur.

The location of cyclones with core pressure below 1000 hPa undergoes a northeastward shift over Europe and the East Atlantic with rising GHG concentrations (Fig. 4c). Increasing numbers are found between the east coast of Greenland and Northern Russia, and locally over Hudson Bay, while the frequency of cyclones further south over the Atlantic and central

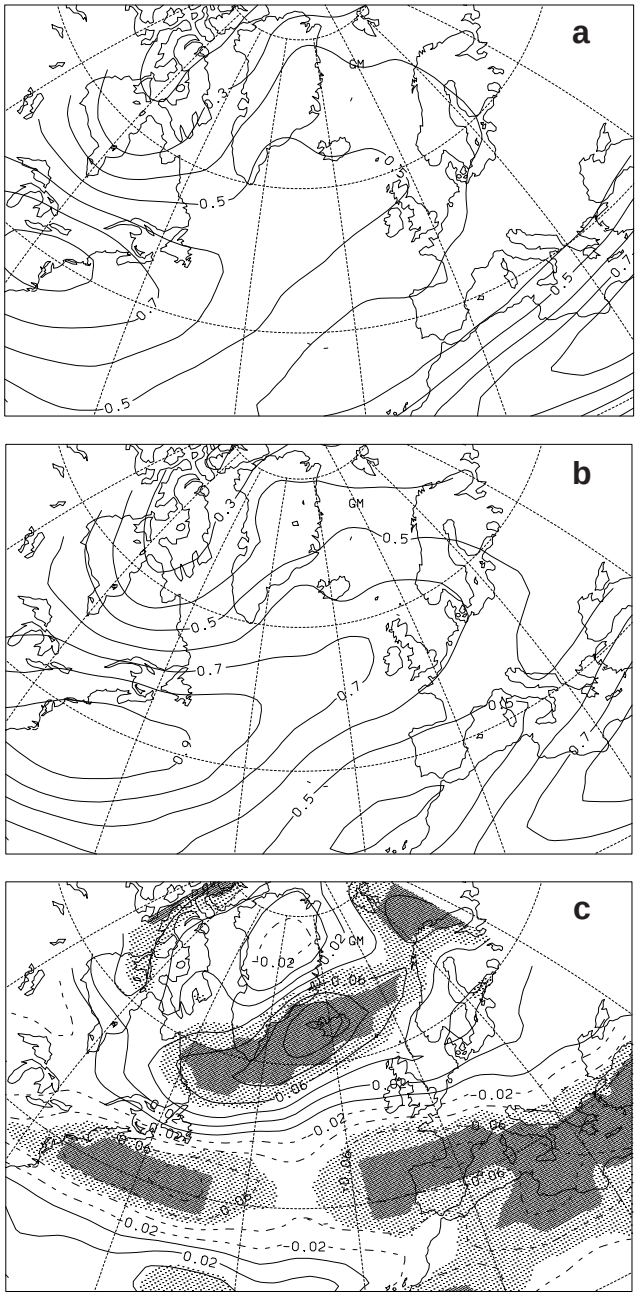

Fig. 3. Winter (DJF) mean maximum Eady growth rate for the 300 to 500 hPa layer. (a) NCEP re-analysis, 1949/50 to 1995/96; (b) control period; and (c) scenario – control period. Isoline spacing is 0.1 d^{-1} in (a) and (b) and 0.02 d^{-1} in (c). Light and dark shading in (c) indicates statistical significance at the 5% and 1% levels, respectively (with respect to a local *t*-test)

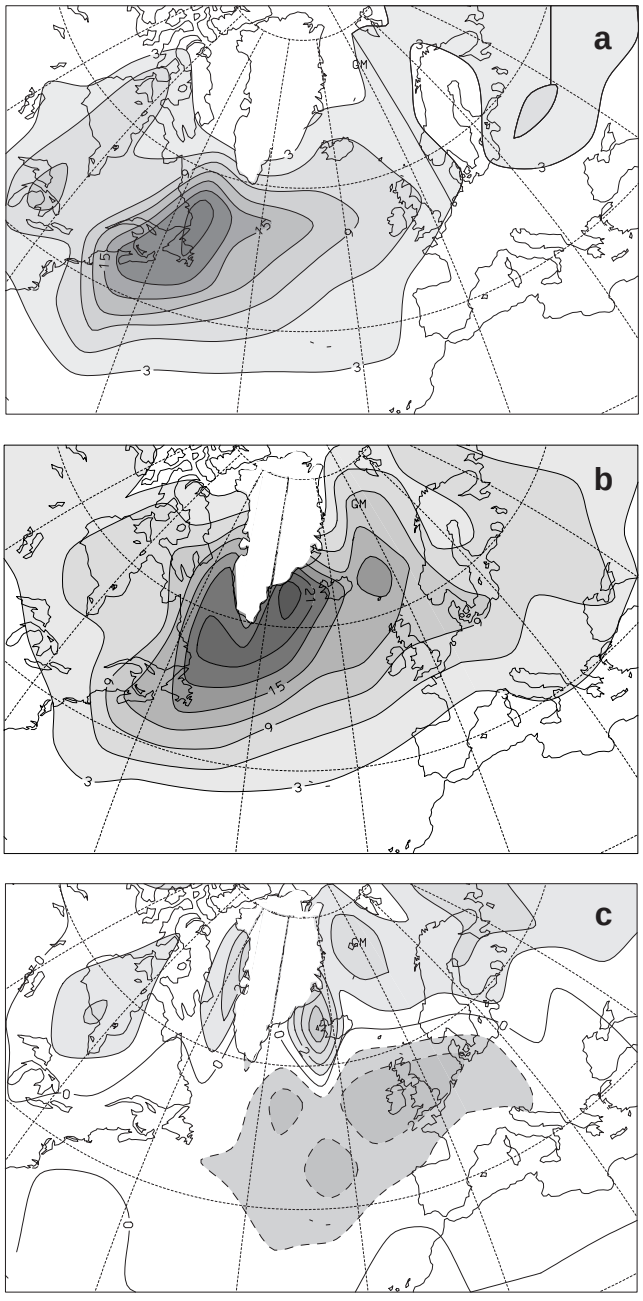

Fig. 4. Mean winter (DJF) frequency of cyclones with core pressures less then 1000 hPa. (a) ECMWF re-analysis, 1978/79 to 1993/94; (b) control period; and (c) scenario – control period. Units are events per winter in a 10° × 10° grid box. Isoline spacing is 3 in (a) and (b) and 1 in (c). In (a) and (b) values greater than 3 and in (c) values greater than 1 and smaller than –1 are shaded

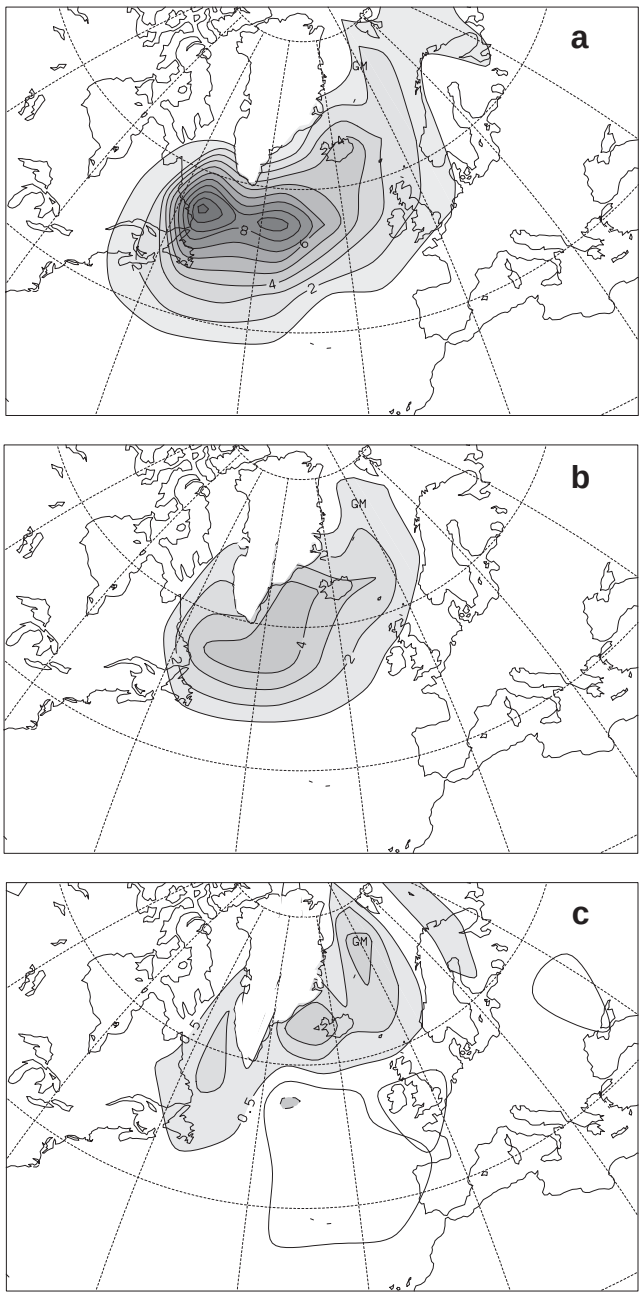

Fig. 5. Mean winter (DJF) frequency of cyclones with core pressures less than 970 hPa. (a) ECMWF re-analysis, 1978/79 to 1993/94; (b) control period; and (c) scenario – control period. Units are events per winter in a 10° × 10° grid box. Isoline spacing is 1 in (a) and (b) and 0.5 in (c). In (a) and (b) values greater than 1 and in (c) values greater than 0.5 and smaller than –0.5 are shaded

Europe is reduced. This leads to negligible changes in the total numbers of cyclones over the whole Atlantic.

For the deep cyclones with core pressures less than 970 hPa (whose occurrence is mainly restricted to the Labrador Sea, the Atlantic north of 50° N and the Norwegian Sea in the control period, Fig. 5b), increasing frequencies at high latitudes are not balanced by decreasing numbers at more southerly locations (Fig. 5c), as would be the case for a pure meridional shift of the pattern. Consequently, the total number of

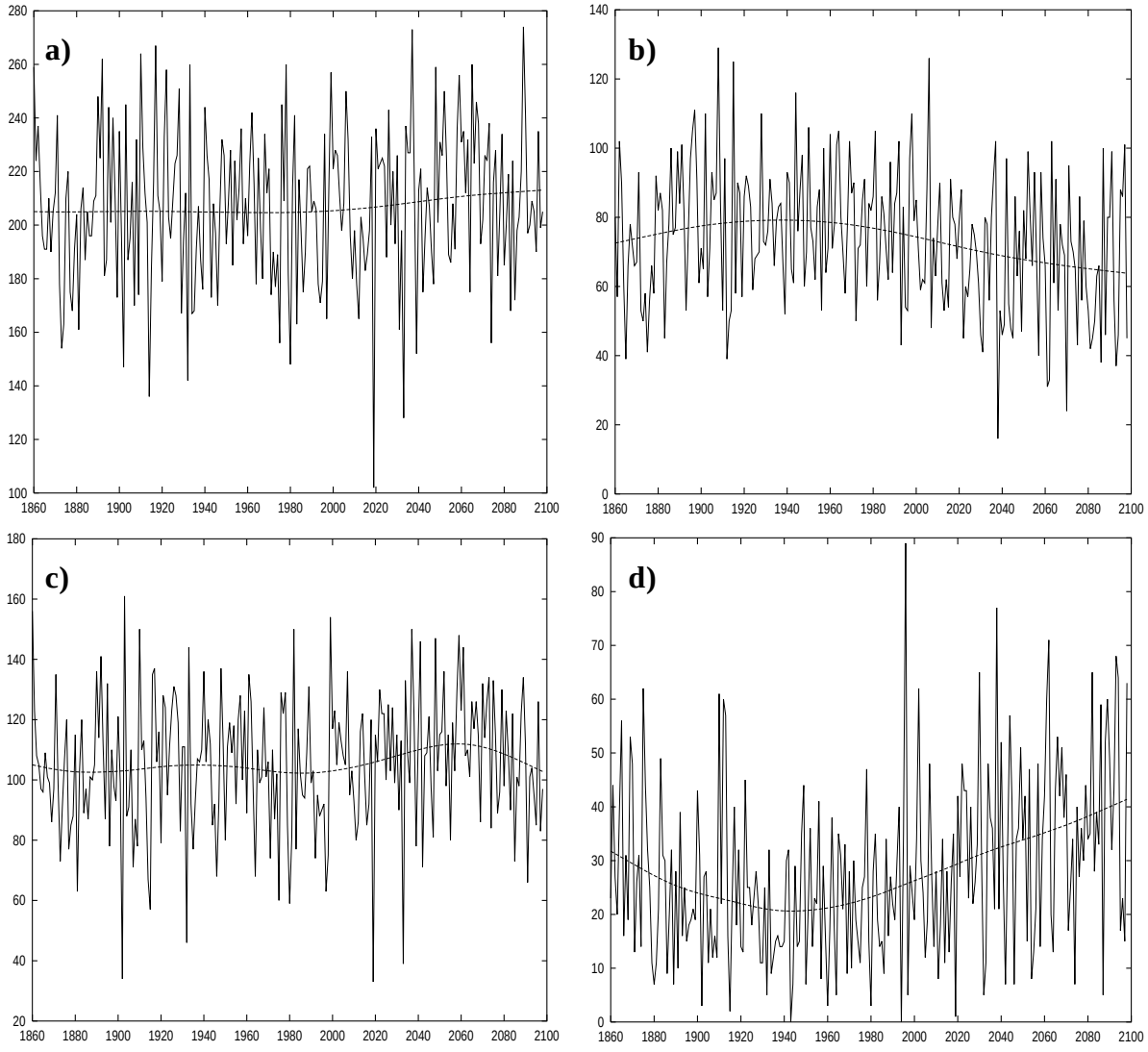

Fig. 6. Time series and nonlinear trends of cyclone frequency (30° W to 30° E, 35° to 80° N). Units are events per winter season (DJF). Core pressure ranges are (a) <1000 hPa, (b) 990–1000 hPa, (c) 970–990 hPa, and (d) <970 hPa

these cyclones over the whole Atlantic increases by about 40 % from 51 events per winter in the control period to 72 during the scenario period. Note that the increase for extreme cyclones (with core pressures less than 950 hPa) from 1.74 to 2.82 events per winter over the Atlantic (+62 %) is even larger (not shown).

A local *t*-test is not suitable for evaluating the statistical significance of the local signals (in 10° × 10° grid boxes) in cyclone frequency because of their non-Gaussian distribution. We therefore calculated time series of cyclone counts per winter over the complete scenario run for a larger window (30° W to 30° E, 35° to 80° N), the area of major changes of cyclone frequency. To exhibit the nonlinear trend we added a spline fit to these figures (see Fig. 6). Kendall's τ (Press et al. 1992) is used to test whether the time series show a statistical significant trend. The results confirm that for this area a small but insignificant increase in the total number of cyclones (with core pressures below 1000 hPa, Fig. 6a) is the result of a decrease in the frequency of shallow cyclones (990 hPa < p_{core} < 1000 hPa, Fig. 6b) and a strong increase in the frequency of deep cyclones (p_{core} < 970 hPa) (Fig. 6d), which is significant at the 1 % level. The intermediate cyclones (970 hPa < p_{core} < 990 hPa, Fig. 6c) do not show significant changes.

3.3. Storm track activity

Upper air storm track activity is computed from the 2.5 to 8 d bandpass-filtered 500 hPa geopotential

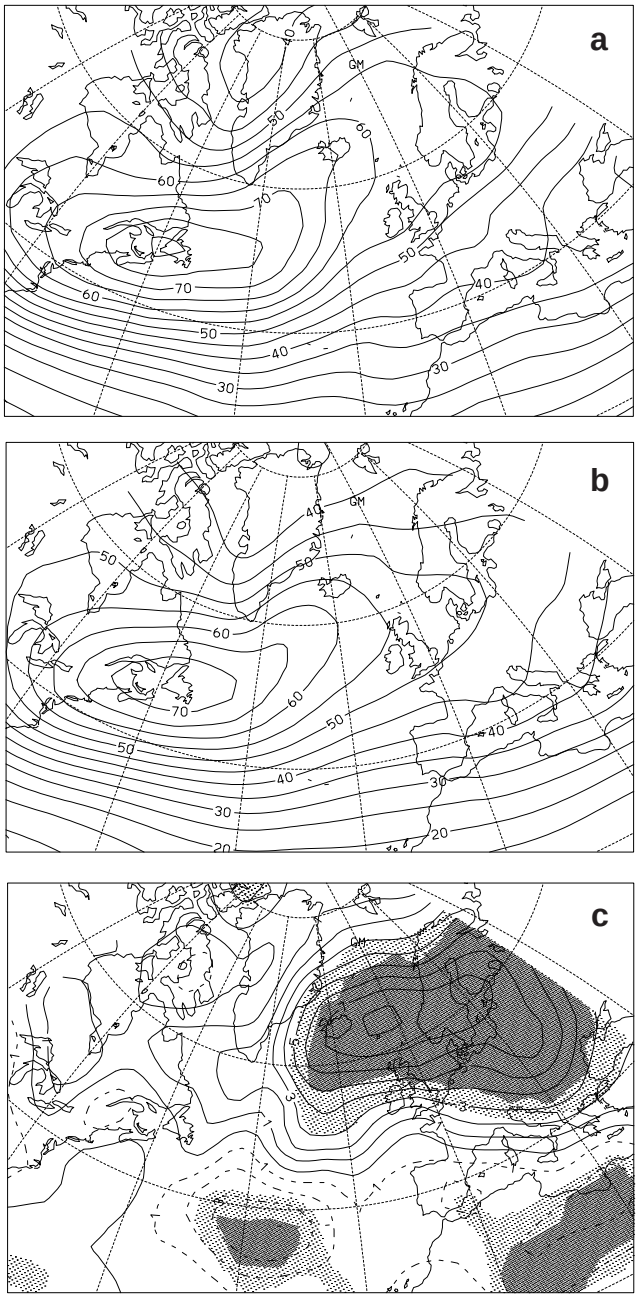

Fig. 7. Winter (DJF) mean storm track activity (2.5 to 8 d band-pass-filtered standard deviation of the 500 hPa geopotential height). (a) ECMWF re-analysis, 1978/79 to 1993/94; (b) control period; and (c) scenario – control period. Isoline spacing is 5 gpm in (a) and (b) and 1 gpm in (c). Light and dark shading in (c) indicates statistical significance at the 5% and 1% levels, respectively (with respect to a local *t*-test)

height standard deviation (see Christoph et al. 1995). The wintertime mean storm track activity calculated from the ECMWF re-analysis for 1978/79 to 1993/94 (Fig. 7a) shows a distinct maximum of about 80 gpm over Newfoundland and a zone of relatively high activity reaching from there over the Atlantic into Northern and Central Europe. A comparison to the winter mean of the control period (Fig. 7b) reveals that the model simulates storm track activity quite well except for a 10% underestimation with regard to the observed values.

One of the most striking features of the climate signal (Fig. 7c) is the increase in storm track intensity over the Eastern North Atlantic and Europe, with a maximum of 8 gpm (increase of 15%) between Iceland and South Norway. This change leads to an extension of the region of high storm track activity further into Northern Europe. A region of decreased storm track activity is located south of 45° N over the Atlantic, the Mediterranean and North Africa with a minimum of about –3 gpm over the Central North Atlantic. Ulbrich & Christoph (1999) argued that there might be a positive feedback between the storm track and the MSLP signal (Fig. 1c) in this climate change experiment.

3.4. Winter mean 10 m wind speed

The winter mean 10 m wind speed averaged over the control period (Fig. 8a) clearly reflects the strong influence of surface roughness in this level. High wind speeds are found over the entire North Atlantic with a maximum of about 12.5 m s^{-1} south of Greenland and a distinct drop along the coastlines. The difference between the scenario and the control period (Fig. 8b) reveals that wind speed increases significantly over Northern Europe as well as over Hudson Bay and the Greenland Sea, whereas decreasing wind speeds can be found over a band reaching from the east coast of the USA into the Mediterranean. The absolute change of up to 0.6 m s^{-1} over Northern Europe corresponds to a relative increase of about 8%. Over the Hudson Bay and the Greenland Sea the relative increases of up to 13 or 17%, respectively, are much higher. The latter signals are connected to a strong decrease in sea-ice cover and will be discussed in Section 5.

In order to assess the time evolution of the wind signal and the relation between the signal and the internal variability, an empirical orthogonal function (EOF) analysis (see e.g. Preisendorfer 1988) over all 240 winter means of the 10 m wind speed of the scenario run was performed following the method presented in Ulbrich & Christoph (1999). Although this study is focused on the North Atlantic/European sector, the EOF analysis is based on global data, since a more regional EOF is too strongly influenced by local variability patterns that might dominate over the GHG trend. The 50 yr low-pass-filtered curve of the resulting first principal component (PC) (Fig. 9a) shows a nearly parallel development compared to the GHG

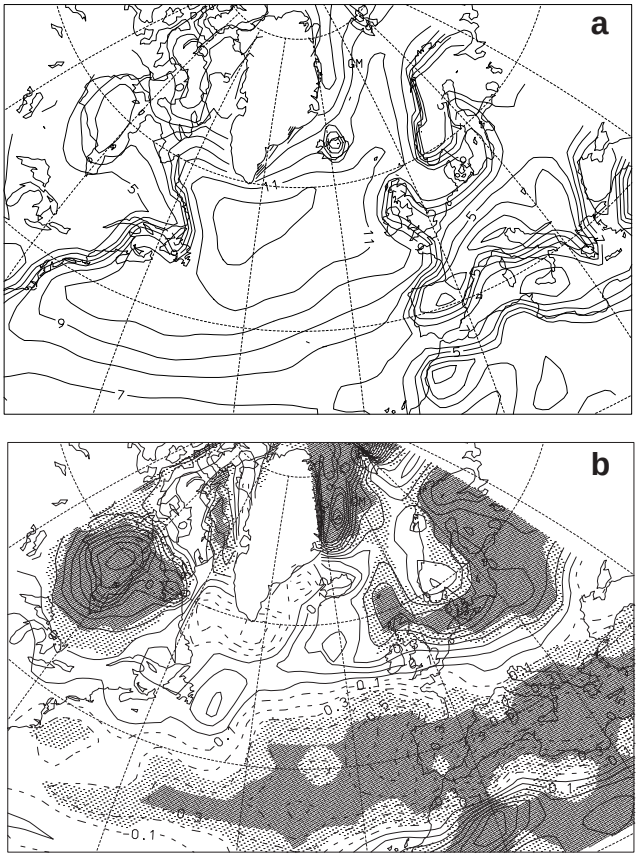

Fig. 8. Winter mean 10 m wind speed. (a) Control period and (b) scenario – control period. Isoline spacing is 1 m s^{-1} in (a) and 0.1 m s^{-1} in (b). Light and dark shading in (b) indicates statistical significance at the 5% and 1% levels, respectively (with respect to a local *t*-test)

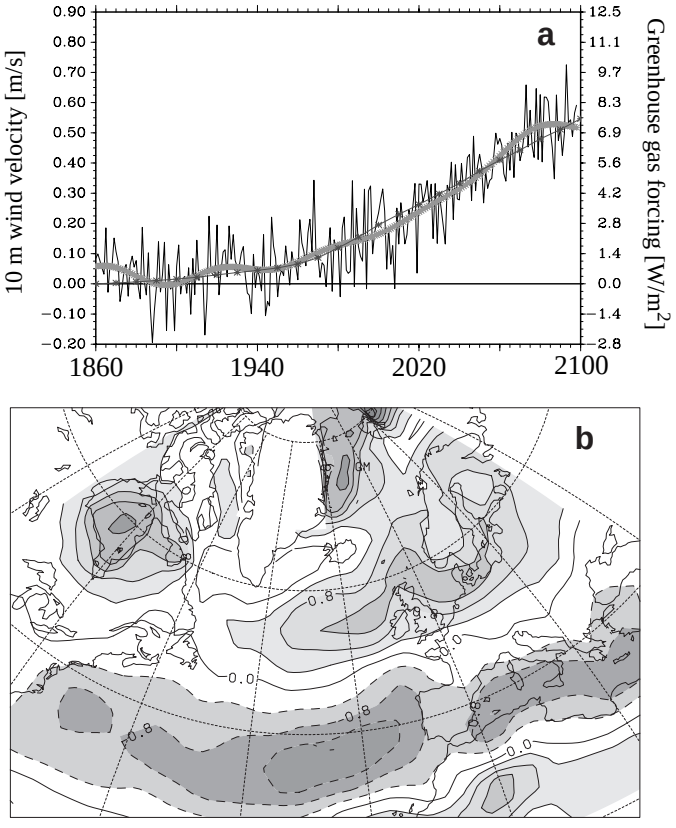

Fig. 9. (a) GHG forcing function (thin grey line) and the first principal component of a global winter mean 10 m wind speed empirical orthogonal function (EOF) for the 240 yr scenario run. The smoothed thick curve is obtained from 50 yr lowpass filtering. (b) The corresponding first EOF (figure is restricted to a Europe/North Atlantic section); isoline spacing is 0.4, with values greater than 0.4 and smaller than –0.4 shaded

forcing function, suggesting that the main features of the GHG signal with respect to 10 m wind speed is captured by the corresponding EOF. The unsmoothed curve reveals a distinct year-to-year variability, whose amplitude, however, is substantially smaller than the magnitude of the GHG trend. The North Atlantic/European sector of the corresponding EOF (Fig. 9b) reproduces the pattern shown in Fig. 8b, underlining that the differences between the control and the scenario period are in fact dominated by the GHG trend rather than by year-to-year variability.

3.5. Wind speed extremes

In order to investigate the changes in wind speed extremes, the upper first percentile of the 12 hourly averaged wind speed was computed for every grid point and for both the control and the scenario 50 winter period. The results for the control period (Fig. 10a) show high similarity to the mean field (Fig. 8a), differing by about a factor of 2 over sea and 2.5 over land. The field of differences between the 2 periods (Fig. 10b) has a similar structure as the signal identified for the mean wind speed, with wind speed extremes increasing over Northern Europe and the adjacent Atlantic as well as over Hudson Bay and the Greenland Sea. There is also a region with strong increases of extreme winds off the east coast of North America. Over the eastern part of the Atlantic west of the Iberian Peninsula and parts of the Mediterranean, wind speed extremes decrease. For most of the regions mentioned the local increases of the upper first percentile are generally somewhat larger than those for mean 10 m wind speed, particularly in the region off the east coast of North America. This can be explained by the increase in wind speed variability on a daily time scale, expressed by the mean intraseasonal stan-

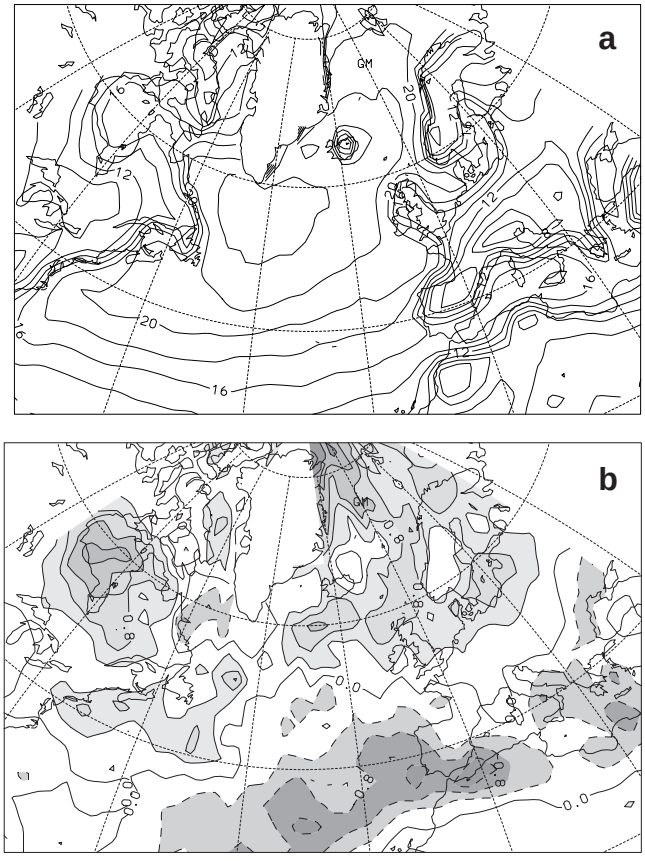

Fig. 10. Upper first percentile of the 10 m wind speed. (a) Control period and (b) scenario – control period. Isoline spacing is 2 m s^{-1} in (a) and 0.4 m s^{-1} in (b), with values greater than 0.4 m s^{-1} and smaller than –0.4 m s^{-1} shaded

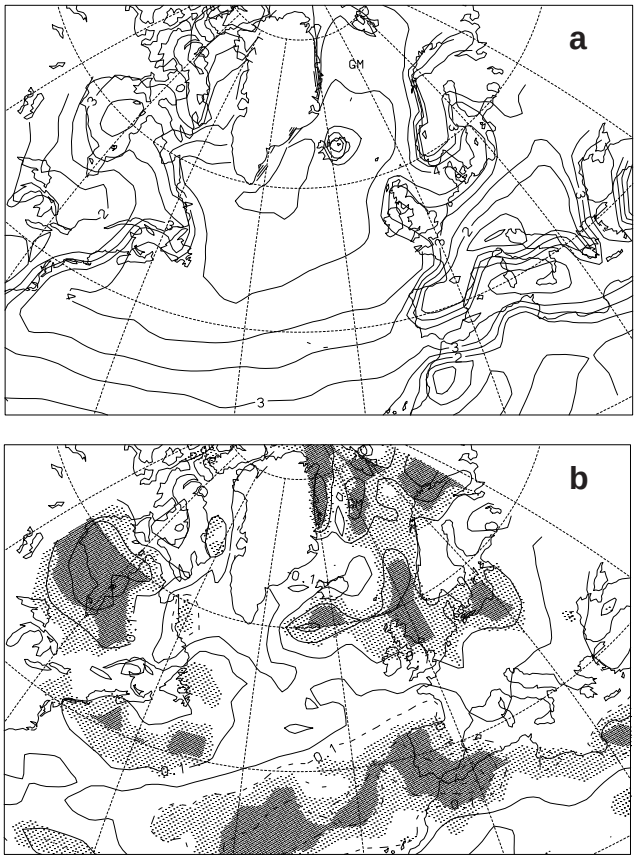

Fig. 11. Mean winter intraseasonal standard deviation of the 10 m wind speed. It was calculated from the 12 hourly data for each winter and then averaged over the whole period. (a) Control period and (b) scenario – control period. Isoline spacing is 0.5 m s^{-1} in (a) and 0.1 m s^{-1} in (b). Light and dark shading in (b) indicates statistical significance at the 5% and 1% levels, respectively (with respect to a local *t*-test)

dard deviation of the 10 m wind speed (Fig. 11, for calculation method see figure caption). Over the Mediterranean, however, the changes in mean (Fig. 8b) and extreme wind speed (Fig. 10b) are of the same order. Except for the extreme western part of the basin, changes in wind speed variability are small (Fig. 11). It can thus be assumed that the reduction of the prevailing mean westerly winds over the central part of the basin (not shown) is the dominant reason for the locally reduced mean and extreme wind speeds.

4. RELATION OF STRONG WIND EVENTS AND CYCLONES

Deep cyclones are often connected with strong pressure gradients on their flanks; which produce extreme wind events. In this section we investigate the relation between the simulated change in deep cyclone occurrence and the regional signal in wind speed over Northern Central Europe. Wind events exceeding local mean plus local day-to-day standard deviation (relative to the 50 winters of the control period) are counted over the whole scenario run for each of 10 grid points over the southern parts of the North and the Baltic Sea (2.8° to 14.1° E, 54.4° to 57.2° N), where a strong signal in the extreme winds was observed (see Section 3.5). For each strong wind event we then looked for the nearest cyclone core, registered the core pressure and grouped them in classes of 10 hPa. The results for the 2 time periods and the 10 grid points mentioned above are presented in Fig. 12. It is striking that nearly all 20 curves reach their maximum in the class between 970 and 980 hPa, revealing that these cyclones are most common for extreme winds at the chosen grid points. Comparing the two 50 winter periods considered, we note that the total number of strong wind events (corresponding to the area under the curves) is much higher in the enhanced GHG climate, which is in

agreement with the results discussed in Section 3.5. Since all curves show a rather similar development for relatively shallow cyclones, this difference is nearly exclusively due to cyclones with core pressures less than 970 hPa, indicating that there is a connection between the increase in extreme winds and the rising number of deep cyclones (see Section 3.2). Note that both changes could (at least partly) be related to the reduction of mean pressure at high latitudes (see Fig. 1c). If we consider lows as minima superposed on a mean pressure field (ignoring their mutual dependence), a reduction of mean pressure would lead to an enhanced number of deep lows. Still, the pressure gradient averaged around the cores of the lows could be unchanged, as in the results of Schubert et al. (1998). The increase of the westerly mean current (caused by the increased mean meridional pressure gradient), however, would then enhance the winds at the southern flanks of the lows and lead to a larger number of extreme wind events.

In addition to that, we also investigated the relationship between mean and extreme winds over Northern and Central Europe (0° to 33.75° E, 51.6° to 68.4° N) and the upper air storm track activity in a slightly larger window (8.4° W to 31.0° E, 40.5° to 71.2° N). The correlation between the 2 area-averaged quantities over the whole 240 yr of the scenario run is 0.66 for the winter means and 0.49 for the winter maxima in 10 m wind speed (determined from the 12 hourly averaged values, see Section 2). This underlines that there is indeed a strong relation between extreme winds and baroclinic activity for Northern and Central Europe, which is reflected by the increase of both quantities in this GHG simulation.

In contrast, over the Mediterranean the reduction in extreme wind speeds is not associated with a marked change in wind speed variability nor in baroclinic activity, and thus the locally reduced westerly mean current (as a consequence of the weakening of the mean pressure gradient) seems to be the dominating factor.

5. WIND SIGNALS AND SEA ICE

We showed in Section 3 that both mean and extreme winds over the Hudson Bay area are strongly increased in the scenario period. This area is isolated from the other regions with strong increases and the changes are mainly restricted to the sea grid points. By looking at the increase of mean zonal wind at different levels (not shown), we found that the signal is restricted to the atmospheric layers below 850 hPa. In contrast, the local changes over the Central European area (see Section 4) are also evident at upper levels.

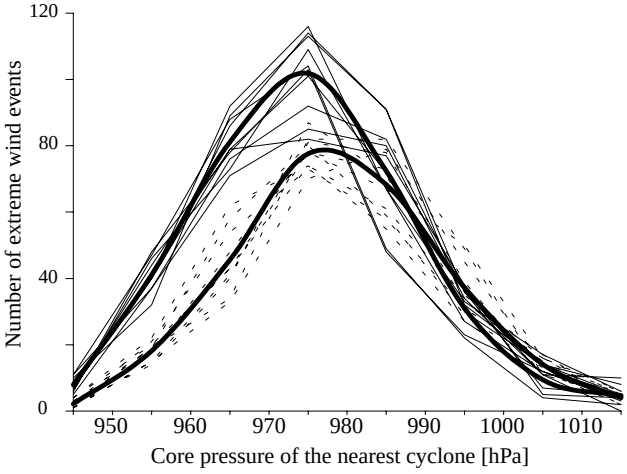

Fig. 12. Number of winter (DJF) storm events (≥2 SD positive anomaly with respect to the 50 winter control period) and the core pressure of the nearest cyclone. Individual curves show distributions for 10 grid points over the North and Baltic Sea (54.4° to 57.2° N, 2.8° to 14.1° E). Dashed lines: control period (1880 to 1930); solid lines: scenario (2039 to 2089). Thick curves: smoothed averages over the 10 grid points

We thus assume that the increase in wind speed over Hudson Bay must be due to changes in the atmospheric boundary layer. The strong rise in low-level temperatures with increasing GHG concentrations (up to 11 K in the 2 m temperature over Hudson Bay) leads to a distinct decrease in winter mean sea-ice cover by about 30 to 50 %. The decreasing static stability connected with the enhanced sensible heat flux from the increasingly ice-free surface and the associated enhanced turbulent transport of momentum from the free atmosphere downward into the planetary boundary layer (PBL) are likely to be the physical mechanisms that produce the wind speed increase. A decrease in (model) surface roughness, which leads to an acceleration of low-level winds, does not contribute much to increasing winds, as model roughness is only reduced when the ocean is completely ice-free over a whole grid box. In spite of the strong reduction this is rarely the case over the model's 'Hudson Bay' in winter. This effect may rather contribute to the increasing wind speed in the Greenland Sea, where the sea-ice disappears over some parts with increasing GHG concentrations. Assuming a logarithmic wind profile, a PBL height of 100 m and further a roughness length of 0.5 mm over sea-ice and 0.015 mm over open water (as used in the ECHAM4), this mechanism might explain about one-third of the 17 % increase of the mean wind speed over the Greenland Sea (see Section 3.4). An additional factor for the increases of extreme winds over Hudson Bay may also be the higher frequency of weak local cyclones (see Fig. 4c).

6. DISCUSSION AND CONCLUSIONS

Synoptic activity and 10 m wind speed over Europe, the North Atlantic and Eastern North America are analysed in a 240 yr transient GHG forcing experiment (according to the IS92a scenario) with the ECHAM4/OPYC3 coupled ocean-atmosphere model at T42 resolution. In summary, the most important changes under the GHG forcing simulated by the model are the folloing: (1) The position of the cyclone cores is shifted north- and eastward over Europe and the Eastern North Atlantic. (2) The number of relatively shallow cyclones over Europe and the Eastern North Atlantic decreases slightly. The number of deep cyclones increases, so that the total number of cyclones changes only insignificantly. (3) Over the Hudson Bay and the Greenland Sea both mean wind speeds and wind speed extremes increase caused by changes in the PBL due to a strong decrease in winter mean sea-ice cover. Over Northern Europe and parts of the Eastern North Atlantic the positive signal in mean and extreme wind speed is caused by an intensification of the westerly mean current and an augmented occurrence of deep cyclones. Over the Mediterranean, where small changes in cyclone frequency were found, decreasing mean and extreme wind speeds are associated with a weakening of the westerly mean current.

The climate signals of MSLP, low-level wind, synoptic activity and baroclinicity have been shown to be consistent with each other. The assignment of the changes to the climate signal rather than long-term variability was shown for 10 m wind velocities on the basis of an EOF analysis. The same had been done by Ulbrich & Christoph (1999) with respect to storm track activity and sea-level pressure for the same model run. There is a close relationship between the cyclone signal and the signal in the 500 hPa storm track. On the one hand both parameters undergo a northeastward shift over the Eastern North Atlantic and Europe, and on the other hand the intensification of the storm track activity over the north of this region can probably be associated with the augmented occurrence of deep cyclones. Furthermore, the changes in storm track activity are in good agreement with the signal in upper-tropospheric baroclinicity, which is located upstream of the storm track signal, indicating that the additional baroclinicity supports the intensification of developing synoptic systems in this region.

Our results agree with many other GCM studies on GHG forcing. This statement refers to the northward shift of the cyclone tracks and the upper air storm track activity over Europe and the North Atlantic (König et al. 1993, Hall et al. 1994, Schubert et al. 1998), and to the increased number of deep and the decreased number of shallow cyclones with increasing GHG concentrations over this region (Lambert 1995, Carnell & Senior 1998). With respect to the storm track over the Northeast Atlantic, an enhancement is also common to many model studies (see also Hall et al. 1994, Lunkeit et al. 1996, Cubasch et al. 1997, Schubert et al. 1998). In agreement with our findings, an increasing occurrence of high wind speeds over the East Atlantic and Europe has been found by Lunkeit et al. (1996) and by Carnell et al. (1996). Corresponding to the findings of Zwiers & Kharin (1998), we find larger wind extremes in the areas where sea-ice retreated. The coincidence of results from quite different model configuration may point to some degree of robustness and reliability. An investigation with an ECHAM4/T106 time-slice experiment revealed that the results of this study are also largely insensitive with respect to changes in the model's horizontal resolution (W. May, Danish Meteorological Institute, pers. comm. 1999). Some of the studies whose results do not agree with ours are based on very short time slices (e.g. Beersma et al. 1997) or on model simulations which have some problems reproducing the observed patterns of baroclinic activity (Zhang & Wang 1997).

The GHG run considered here does not take into account the effects of anthropogenic changes in sulphur aerosols. Transient climate change experiments including these effects show that in winter the cooling due to aerosols merely leads to a reduction of the temperature response to carbon dioxide (Mitchell & Johns 1997, Roeckner et al. 1998). One may expect that the climate signal in the synoptic activity is also weakened by this additional effect. It is still important to perform the climate change investigations with GHG forcing only. A sensitivity experiment with the HadCM2 model revealed that the weakening influence of sulphur aerosols on GHG induced global temperature rise vanishes within 1 decade after their removal during the continuing transient simulation (T. Johns, Hadley Centre, pers. comm. 1999).

We would like to emphasize that, in spite of a certain agreement between different models, considerable insecurity about their results remains. While some of the mechanisms leading to the changes are evident (the increase in upper air baroclinicity, increasing latent heat release within the baroclinic waves adding to their energy, see Hoffmann 1999 and Cubasch et al. 1999), the apparently most important effect, the increasing number of deep cyclones at the cost of shallow cyclones, has to be carefully investigated in order to exclude the possibility of an artifact of the GCMs. It is not clear whether secondary lows or short-wave disturbances and their importance for the generation of extreme wind events are simulated realistically enough.

Another problem regarding the interpretation of climate change studies arises from the resolution of cli-

mate models, which affects the representation of orography, the land-sea distribution, etc., and consequently the wind signal. We will have to wait for improvements in the nesting of high resolution regional models in order to obtain a more reliable estimate of the local impacts of climate change with respect to extreme wind events.

Acknowledgements. We would like to thank the anonymous reviewers for their detailed comments that helped to improve the manuscript. This work was partially supported by the Deutsche Forschungsgemeinschaft within Sonderforschungsbereich (SFB) 419 and by the Federal German Ministry of Research (BMBF) under grant No. 01 LA9861/5.

LITERATURE CITED

Bacher A, Oberhuber MJ, Roeckner E (1998) ENSO dynamics and seasonal cycle in the tropical Pacific as simulated by the ECHAM4/OPYC3 coupled general circulation model. Clim Dyn 14:431–450

Beersma JJ, Rider KM, Komen GJ, Kaas E, Kharin VV (1997) An analysis of extra-tropical storms in the North Atlantic region as simulated in a control and 2 × CO_2 time-slice experiment with a high-resolution atmospheric model. Tellus 49A:347–361

Carnell RE, Senior CA (1998) Changes in mid-latitude variability due to increasing greenhouse gases and sulphate aerosols. Clim Dyn 14:369–383

Carnell RE, Senior CA, Mitchell JFB (1996) An assessment of measures of storminess: simulated changes in northern hemisphere winter due to increasing CO_2. Clim Dyn 12: 467–476

Christoph M, Ulbrich U, Haak U (1995) Faster determination of the intraseasonal variability of storm tracks using Murakami's recursive filter. Mon Weather Rev 122:578–581

Cubasch U (ed), Caneill JY, Filiberti MA, Hegerl G, Johns TC, Keen A, Parey S, Thual O, Ulbrich U, Voss R, Waszkewitz J, Wild M, van Ypersele JP (1997) Anthropogenic climate change. Project No. EV5V-CT92–0123 final report. Office for Official Publications of the European Comission No. EUR 17466EN, Luxembourg

Cubasch U, Allen M, Beniston M, Bertrand C, Brinkop S, Caneill JY, Dufresne JL, Fairhead L, Filiberti MA, Gregory J, Hegerl G, Hoffmann G, Johns T, Jones G, Laurent C, McDonald R, Mitchell J, Parker D, Oberhuber J, Poncin C, Sausen R, Schlese U, Stott P, Tett S, leTreut H, Ulbrich U, Valcke S, Voss R, Wild M, Ypersele JP (1999) Summary Report of the Project Simulation, Diagnosis and Detection of the Anthropogenic Climate Change (SIDDACLICH). ENV4-CT95–0102. Office for Official Publications of the European Commission No. EUR 19310, Luxembourg

Dorland C, Tol RSJ, Olsthoorn AA, Palutikof JP (1996) An analysis of storm impacts in the Netherlands. In: Downing TE, Olsthoorn AA, Tol RSJ (eds) Climatic change and extreme events. ECU-Research Report Number 12, VU Boekhandel/Uitgeverij, Amsterdam, p 157–184

Dronia H (1991) On the accumulation of excessive low pressure systems over the North Atlantic during the winter seasons (November to March) 1988/89 to 1990/91. Die Witterung in Übersee 39:27

Eady ET (1949) Long waves and cyclone waves. Tellus 1: 33–52

Fantini M (1993) A numerical study of two-dimensional moist baroclinic instability. J Atmos Sci 50:1199–1210

Golding B (1984) A study of the structure of mid-latitude depressions in a numerical model using trajectory techniques. I: Development of ideal baroclinic waves in dry and moist atmospheres. Q J R Meteorol Soc 110:847–879

Gutowski WJ, Branscome LE, Stewart DA (1992) Life cycles of moist baroclinic eddies. J Atmos Sci 49:306–319

Haak U, Ulbrich U (1996) Verification of an objective cyclone climatology for the North Atlantic. Meteorol Z 5:24–30

Hall NMJ, Hoskins BJ, Valdes PJ, Senior CA (1994) Storm tracks in a high-resolution GCM with doubled carbon dioxide. Q J R Meteorol Soc 120:1209–1230

Held IM (1993) Large scale dynamics and global warming. Bull Am Meteorol Soc 74:228–241

Held IM, O'Brien EO (1992) Quasigeostrophic turbulence in a Three-Layer-Model: effects of vertical structure in the mean shear. J Atmos Sci 49:1861–1870

Hoffmann G (1999) Die Bedeutung der diabatischen Heizung für die synoptische Störungsaktivität der Nordhemisphäre im heutigen und in einem zukünftigen Klima. In: Ebel A, Kerschgens M, Neubauer FM, Speth P (eds) Mitteilungen aus dem Institut für Geophysik und Meteorologie der Universität zu Köln. University of Cologne

Hoskins BJ, Valdes PJ (1990) On the existence of storm-tracks. J Atmos Sci 47:1854–1864

IPCC (1992) Climate change 1992: the supplementary report to the IPCC scientific assessment. Cambridge University Press, Cambridge

IPCC (1996) Climate change 1995: the science of climate change. Cambridge University Press, Cambridge

Kaas E, Li TS, Schmith T (1996) Statistical hindcast of wind climatology in the North Atlantic and northwestern European region. Clim Res 7:97–110

Karoly DJ, Cohen JA, Meehl GA, Mitchell JFB, Oort AH, Stouffer RJ, Wetherald RT (1994) An example of fingerprint detection of greenhouse climate change. Clim Dyn 10:97–105

König W, Sausen R, Sielmann F (1993) Objective identification of cyclones in GCM simulations. J Clim 6:2217–2231

Lambert SJ (1995) The effect of enhanced greenhouse warming on winter cyclone frequencies and strength. J Clim 8: 1447–1452

Lambert SJ (1996) Intense extratropical Northern Hemisphere winter cyclone events: 1899–1991. J Geophys Res 101:21319–21325

Lindzen RS, Farrel B (1980) A simple approximate result for the maximum growth rate of baroclinic instabilities. J Atmos Sci 37:1648–1654

Lunkeit F, Ponater M, Sausen R, Sogalla M, Ulbrich U, Windelband M (1996) Cyclonic activity in a warmer climate. Beitr Phys Atmos 69:393–407

Lunkeit F, Fraedrich K, Bauer SE (1998) Storm tracks in a warmer climate: sensitivity studies with a simplified global circulation model. Clim Dyn 14:813–826

Machenhauer B, Windelband M, Botzet M, Hesselbjerg-Christensen J, Deque M, Jones RG, Ruti PM, Visconti G (1998) Validation and analysis of regional present-day climate and climate-change simulations over Europe. Report No. 275, Max-Planck-Institut für Meteorologie, Hamburg

Mengelkamp HT (1999) Wind climate simulation over complex terrain and wind turbine energy output estimation. Theor Appl Climatol 63:129–139

Mitchell JFB, Johns TC (1997) On the modification of global warming by sulphate aerosols. J Clim 10:245–267

Mitchell JFB, Manabe S, Tokioka T, Meleshko V (1990) Equi-

librium climate change. In: Houghton JT, Jankins GJ, Ephraums JJ (eds) Climate change, the IPCC scientific assessment. Cambridge University Press, Cambridge, p 131–172

Munich Re (1977) Der Capella-Orkan. Januarstürme 1976 über Europa. Münchener Rückversicherungs-Gesellschaft

Munich Re (1990) Sturm—Neue Schadendimensionen einer Naturgefahr. Münchener Rückversicherungs-Gesellschaft

Oberhuber JM (1993) Simulation of the Atlantic circulation with a coupled sea ice-mixed layer-isopycnal general circulation model. Part I: Model description. J Phys Oceanogr 22:808–829

Pavan V (1996) Sensitivity of a multi-layer, quasi-geostrophic β-channel to the vertical structure of the equilibrium meridional temperature gradient. Q J R Meteorol Soc 122: 55–72

Penning-Rowsell E, Handmer J, Tapsell S (1996) An analysis of storm impacts in the Netherlands. In: Downing TE, Olsthoorn AA, Tol RSJ (eds) Climatic change and extreme events. ECU-Research Report Number 12, VU Boekhandel/Uitgeverij, Amsterdam, p 97–127

Preisendorfer RW (1988) Principal component analysis in meteorology and oceanography. In: Mobley CD (ed) Developments in atmospheric science, Vol 17. Elsevier, Amsterdam

Press WH, Teukolsky SA, Netterling WT, Flannery BP (eds) (1992) Numerical recipes in FORTRAN, 2nd edn. Cambridge University Press, Cambridge, p 488–494

Roeckner E, Arpe K, Bengtsson L, Dümenil L, Esch M, Kirk E, Lunkeit F, Ponater M, Rockel B, Sausen R, Schlese U, Schubert S, Windelband M (1992) Simulation of present-day climate with the ECHAM model: impact of model physics and resolution. Report No. 93, Max-Planck-Institut für Meteorologie, Hamburg

Roeckner E, Arpe K, Bengtsson L, Christof M, Claussen M, Dümenil L, Esch M, Giorgetta M, Schlese U, Schulzweida U (1996a) The atmospheric general circulation model ECHAM4: model description and simulation of present-day climate. Report No. 218, Max-Planck-Institut für Meteorologie, Hamburg

Roeckner E, Oberhuber JM, Bacher A, Christof M, Kirchner I (1996b) ENSO variability and atmospheric response in a global coupled atmosphere-ocean GCM. Clim Dyn 12: 737–754

Roeckner E, Bengtsson L, Feichter J, Lelieveld J, Rhode H (1998) Transient climate change simulations with a coupled atmosphere-ocean GCM including the tropospheric sulfur cycle. Report No. 266, Max-Planck-Institut für Meteorologie, Hamburg

Schinke H (1993) On the occurrence of deep cyclones over Europe and the North Atlantic in the period 1930–1991. Beitr Phys Atmos 66:223–237

Schmith T, Kaas E, Li TS (1998) Northeast Atlantic winter storminess 1875–1995 re-analysed. Clim Dyn 14:529–536

Schraft A, Durand E, Hausmann P (1993) Storms over Europe: losses and scenarios. Swiss Reinsurance Company, Zürich

Schubert M, Perlwitz J, Blender R, Fraedrich K, Lunkeit F (1998) North Atlantic cyclones in CO2-induced warm climate simulations: frequency, intensity and tracks. Clim Dyn 14:827–837

Stein O, Hense A (1994) A reconstructed time series of the number of extreme low pressure events since 1880. Meteorol Z NF 3:43–46

Stephenson DB, Held IM (1993) GCM response of northern winter stationary waves and storm tracks to increasing amounts of carbon dioxide. J Clim 6:1859–1870

Ulbrich U, Christoph M (1999) A shift of the NAO and increasing storm track activity over Europe due to anthropogenic greenhouse gas forcing. Clim Dyn 15:551–559

von Storch H, Guddal J, Iden KA, Jonsson T, Perlwitz J, Reistad M, de Ronde J, Schmidt H, Zorita E (1993) Changing statistics of storms in the North Atlantic? Report No. 116, Max-Planck-Institut für Meteorologie, Hamburg

WASA-Group (Waves and Storms in the North Atlantic) (1998) Changing waves and storms in the Northeast Atlantic. Bull Am Meteorol Soc 79:741–760

Zhang Y, Wang WC (1997) Model-simulated northern winter cyclone an anticyclone activity under a greenhouse warming scenario. J Clim 10:1616–1634

Zwiers FW, Kharin VV (1998) Changes in the extremes of the climate simulated by the CCC GCM2 under CO_2 doubling. J Clim 11:2200–2222

Editorial responsibility: Hans von Storch, Geesthacht, Germany

Submitted: October 7, 1999; Accepted: January 24, 2000
Proofs received from author(s): May 22, 2000